Empirical Modelling of Surface Currents for Maritime Operations

Yadan Mao[1, 2, 3], Mal Heron[2, 3] and Peter Ridd[1, 2, 3]
1. School of Maths Physics & IT, James Cook University
2. Marine Geophysical Laboratory, James Cook University
3. AIMS @ JCU

Abstract
The urgent nature of search and rescue operations in coastal areas requires a rather precise prediction of surface currents in a timely manner. Given the relatively long running time of numerical hydrodynamic models, they may not be appropriate for use in operational use. Hence, a faster model is desirable and HF ocean surface radar can be applied to solve this problem. An example is given to demonstrate the process by using historical surface current data from an area in Bass Strait collected by HF ocean surface radar. Tidal analysis shows that the significance of tides varies greatly with the location. Variability ellipse analysis reveals the response of surface currents to relatively strong wind from different directions at each grid point. Finally, a fast empirical model is established based on the physical process calibrates the response of surface currents to winds and tides respectively. Residual currents are shown to be small and noisy compared to the observed currents from HF radar. The effects of geostrophic currents and mesoscale eddies do not appear above the noise.

1. Introduction

The surface current in coastal area is more complex than in the open sea. More factors play significant roles in the water dynamics, such as bottom friction, bathymetry variation, constraint on water movement imposed by the coastline, and water flowing trough the entrance of rivers or bays. Therefore, surface currents near the entrance of Port Phillip Bay are expected to vary with location. Densely spaced data with fast repetition are required for detailed study of currents at different locations. In this sense, HF radar is an ideal instrument for current research and maritime operations in coastal area.

The aim of this study is to build up an operational physical empirical model using the historical current data from HF radar, so that with the predicted wind and the astronomical tides, the current at that site can be predicted quickly and with acceptable accuracy. The crucial point in establishing this empirical model is to ascertain the response of surface currents to wind from all directions and at all magnitude. Our study (Mao and Heron 2006) has shown that the response of surface currents to wind is very sensitive to the wind fetch. Both the ratio of current speed to wind speed and the angle between the current vector and the wind vector varies with the fetch.

By using the historical current data near Bass Strait, this paper provides an example of how the model is established. The method explained here can be applied to any place where there is a long enough historical record of surface current data. Search and rescue operations in the coastal area will benefit from the fast predictability of the model.

2. Experiment

The experiment was configured around a phased array HF radar system operating at 30 MHz. It is the COSRAD system, which uses an eight-element antenna array for both transmit and receive modes. A pulse modulation is used and a transmit/receive switch is used to switch from a high energy transmit pulse to a low noise receiver after each transmit pulse. The radar stations were set up at Portsea Backbeach (longitude 144° 42' 16.9"E and latitude 38° 20' 03.6"S) and Ocean Grove (longitude 144° 31' 01.4"E and latitude 38° 16' 20.1"S) in Bass Strait, near the entrance of Port Phillip Bay in Victoria, Australia. The area in which surface current maps are produced ranges from 38.3°S to 38.5°S latitude, 144.5°E to 144.7°E longitude, with the grid points shown as asterisks in Fig. 1. The bathymetry in the near coastal zone is shown in Figure 1. The radar data archive consists of surface current vectors every hour at each of 269 grid points within this area for one month period, from 27 June 2001 to 26 July 2001. Over the 30-day duration, only one hourly data set was lost due to environmental reasons.

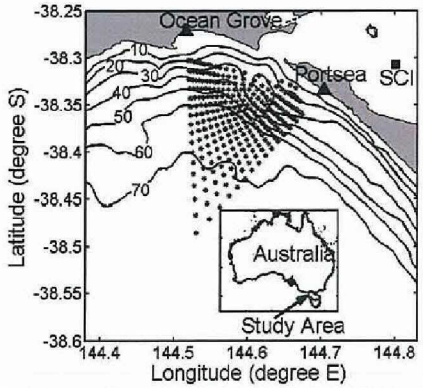

Fig 1 Map of the study area, land (shaded), data grid point (asterisks) and bathymetry contours in metres, two radar stations are marked as triangles, weather station SCI is marked as square.

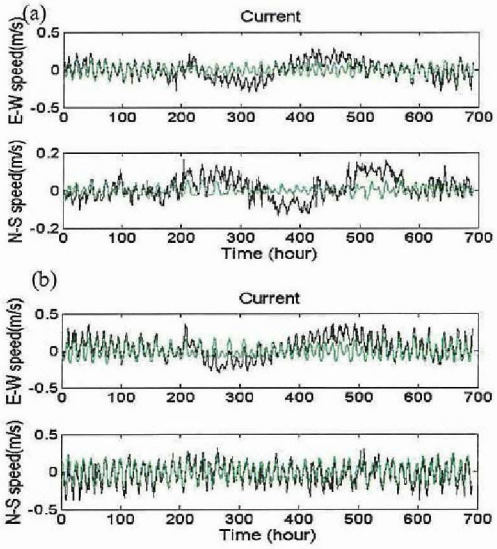

Fig 2 Time series of total current (dark line) and reconstructed tidal current (light line) at a grid point in the southern part (a) and a grid point near the entrance of bay (b). Reference time is 5pm on 27 June 2001 Australian Eastern Standard Time.

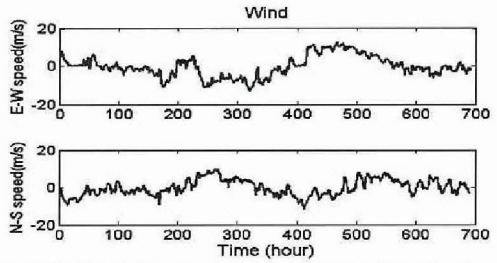

Fig 3 Wind data from an anemometer located on South Channel Island (SCI), reference time is 5pm on 27 June 2001 Australian Eastern Standard Time.

Currents in the study area are mainly driven by tides and winds. Fig. 2 shows typical time series of current components at two of the grid points, one is at the southern part of the study area (Fig 2 (a)), and the other is close to the coast and on the western side of the entrance to the bay (Fig 2 (b)).

It is shown that the strength of tidal signals is different in different parts of the area, especially in the N-S direction: for grid points near the entrance of the bay, the diurnal and semi-diurnal tidal signal is quite strong, while for grid points far from the coast, the tidal signal is much weaker and less obvious. In the East-West direction, diurnal and semi-diurnal tidal signals are obvious in records at both points, though the signal is stronger at the site near to the bay than at the site far from the bay. Wind data are available from an anemometer located 10m above sea level on South Channel Island (marked as SCI in Fig 1). This is the weather station nearest to our research area. Hourly wind data were taken for the 30-day period and the raw values are shown in Fig 3.

Comparing current records in Fig 2 (a) and Fig 2 (b) with wind records in Fig 3, we can see that the low frequency variation of the currents is highly correlated with low frequency variation of the wind. Detailed study on current response to wind in this area confirms this (Mao and Heron 2006).

It is shown in Fig 3 that the high frequency variation of wind records in the N-S direction is stronger than in the E-W direction. Fig 2(a) and Fig 3 suggest that in the southern area the N-S currents are much more influenced by winds than by tides. The high frequency variation of winds interacts with the tidal signal, which results in the less clarity of tidal signal in the N-S current record (Fig 2(a)). On the contrary, tidal signal is strong in the E-W direction, and wind is less variable in this direction, thus the tidal signal is quite clear in the E-W direction for most areas.

3. Currents generated by tides

By using the algorithm of Pawlowicz (2002), we conducted tidal analysis for the filtered current data at each grid point. The length of the current records (1 month) is not long enough for the tidal analysis to differentiate the low frequency variation generated by other non-tidal factors, and since the low frequency variation of current is highly correlated with the wind, surface currents are passed through a high pass filter before the tidal analysis is carried out. Results show that K1 and M2 are the two most dominant tidal components, representing the diurnal and semidiurnal current variation respectively.

In order to show the tidal ellipses of K1 and M2, we chose 38 uniformly distributed points within the radar coverage area. Currents at these points are derived by interpolation. Fig 4 shows the analysed tidal ellipses of K1 and M2 at these uniformly distributed points. The centres of the ellipses are the newly interpolated grid points for which the tidal ellipses are shown. Tidal currents at these points rotate around the ellipse. The '+' and '•' in Figure 4 represent the initial phase of the ellipses: '+' means clockwise rotation, while '•' means anticlockwise rotation. The M2 tidal component rotates anticlockwise in most parts of the area, while the K1 component rotates clockwise on the western side and anticlockwise on the eastern side of the grid pattern.

It is shown that over the entire area, the M2 component is about twice as strong as the K1 component. Tidal currents are strong near the entrance of the Bay with much larger tidal ellipses there than in other areas. For the M2 component, the tidal current near the entrance of the Bay is stronger in the N-S direction as the major axis of the ellipse there is close to the N-S direction, while the reverse is true for tidal currents in other areas. Furthermore, the eccentricities of tidal ellipses near the entrance of the Bay are smaller than other areas, which imply tidal currents

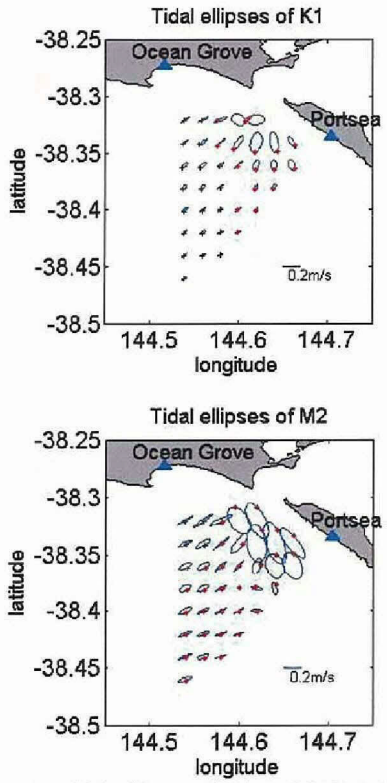

Fig 4 Tidal ellipses of K1 and M2, '+' and '•' represent the initial phase of the ellipses, '+' means clockwise rotation, while '•' means anti-clockwise rotation.

there are more rotational, while tidal currents at other areas are more rectilinear.

We reconstruct tidal current at each grid point using the parameters derived from tidal analysis and calculate the percentage of current variability explained by tides. Records of the reconstructed tidal currents at two typical points are shown in Fig 2. Fig 5 shows the contour of percentage of variability explained by tides. Overall, near the coastal area, tides explain a larger percentage of variability, especially near the entrance to the Bay, where more than 50% of the variability is explained by tides. In the middle and south-eastern area, tides explain the less than 15% variability. This is consistent with the size of ellipse in Fig 4. Fig 5 also shows the percentage of variability explained by tides for the N-S and the E-W current components separately. These results are in agreement with the directions of the major axis of the ellipse shown in Fig 4. More current variability is explained by tides in the direction of the major axis of the tidal ellipses.

It is worth noting that in areas nearest to the entrance to the Bay, the radar measurement is least accurate in the N-S direction, since the two radar stations and the grid point are almost in line; hence little information is

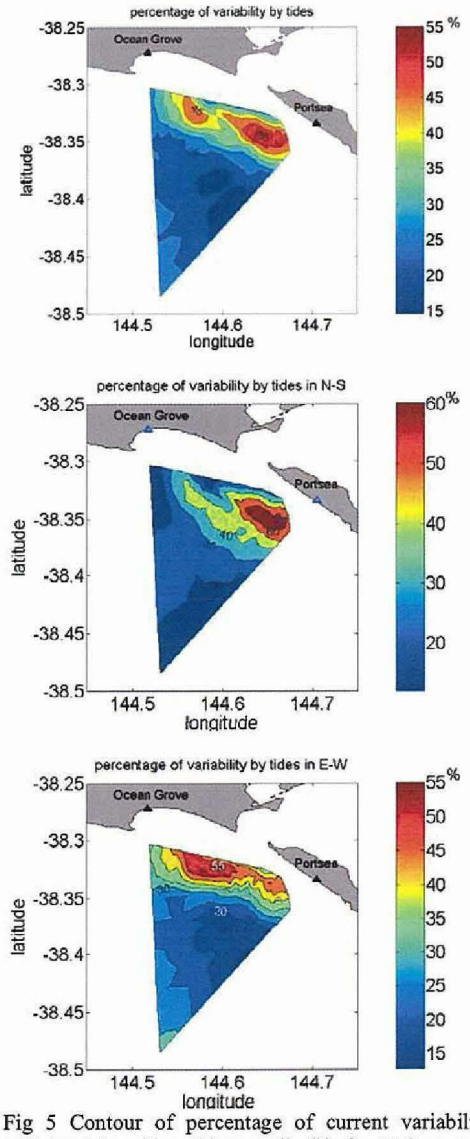

Fig 5 Contour of percentage of current variability explained by tides, (a) overall, (b) for N-S current component, (c) for E-W current component

given in the N-S direction. Indeed we found the current records for grid points just next to the entrance of the Bay are quite noisy in the N-S direction, and both the tidal signal and low frequency current generated by wind are not clear on the record. This is why in Fig 6 (b), tides explain much less variability in the area nearest to the entrance than in the area a little further away and to the east of entrance. It also explains why in Fig 6 (b), the current is least correlated with the wind in the area nearest to the entrance.

4. Currents generated by winds

The response of surface currents to wind has two

components: surface currents caused by momentum transfer through wind shear stress, and the Stokes mass transport. The former is governed by a quadratic law and explained by Ekman theory; the latter is governed by a linear law and caused by the non-linear character of waves generated by wind. These two laws are independent of each other, but work together to generate the response of the current to the wind. In different conditions, they play different roles.

Resolving wind and wave-drift components from each other and from a larger scale main flow is a difficult experimental problem. Most laboratory and field investigations have focused on just one component (Kirwan, 1979).

In most numerical modelling of ocean currents, the effect of Stokes drift is often not considered and the knowledge about wind stress is inadequate. These would cause significant errors in the results. Recent studies (Lewis, Belcher 2003, Polton, Lewis et al, 2005) suggest that by adding the influence of Stokes drift into the Ekman model, the analytical solutions agree better with current profiles from previously published observation data than when the standard Ekman model is used on its own.

Based on this set of current and wind data, the relation between the surface currents and the wind in this area is studied in detail in another paper (Mao and Heron 2006). By incorporating both the Ekman-type current and the Stokes drift into the wind response model, our study (Mao and Heron 2006) indicates that fetch significantly influences the total response of surface currents to wind. Both the magnitude and direction of current response varies with the wind fetch, due to the coupling of wind to Stokes drift at different stages of sea state development.

As the low frequency variation of the current is highly correlated with the wind, both the current and the wind are filtered by a 25-hour boxcar filter before the analysis. In order to ascertain the angle relation between the current and the wind over the whole time series, we vary the angle values and conduct the correlation analysis. The angle values shown in Figure 6 (a) are the values that correspond to the highest correlation coefficient (Figure 6(b)) between the current and the wind. The angle is defined in a way that positive means the current is to the left of the wind. For most of the area, the value ranges between 10° to 45°, which is in agreement with other observational results (Huang, 1979). Near the coast, where the current is subject to more factors (constraint by the coastline, flows from the Bay, more significant bottom friction effect), the angle is out of this range. It is shown in Figure 6(b) that, except for areas near the entrance of the bay, the filtered current is highly correlated with the wind for most of study area, with correlation coefficient around 0.8.

The response of currents to wind varies with location. A typical current response to wind at a specific time is

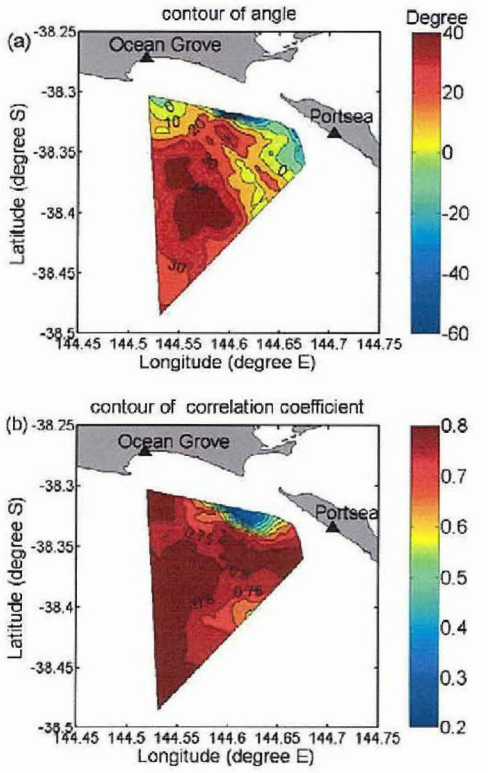

Fig 6 Contour of relation between the surface current and the wind over the whole period (a) angle between current and wind (positive value means current is to the left of the wind) (b) Correlation coefficient

shown in Fig 7. Near the entrance of the Bay, currents are influenced by flows out of the Bay. Near the coast, where the influence of bottom friction is strong, currents tend to follow the direction of the wind. Due to large variation in bathymetry gradient around the 60m-bathymetry line, currents in the middle area are steered along the bathymetry line. In the southern part, due to effect of Coriolis force, current vectors are on the left side of the wind vector. Apart from location, the response of surface currents to wind also varies with wind fetch and duration (Mao and Heron 2006). Therefore the response of surface currents to wind has to be studied with respect to both the current location and the wind condition.

5. Empirical model for currents

The time series records of filtered currents at each grid point and filtered winds are separated into different sections according to wind direction. Wind records with amplitude less than 3m/s are negligible since the influence on currents is quite limited. Wind of similar directions in the time series fall into a section, and currents are correlated with the wind for each section.

For each section, variability ellipses were obtained at each grid point. Fig 8 shows the typical variability ellipses of two sections: under long fetch wind conditions and short fetch conditions. The major axis

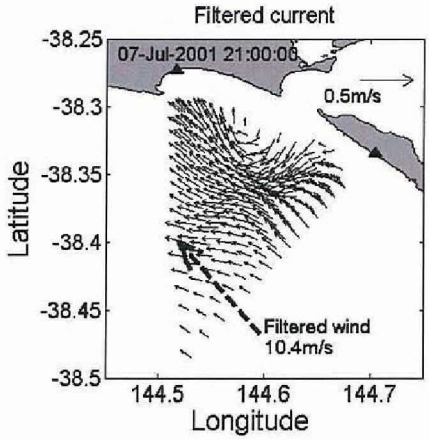

Fig 7 Filtered surface currents and filtered wind at a specific time. The dashed arrow represents wind direction. Current speed is indicated by the scale on the top, and wind speed is 10.4m/s.

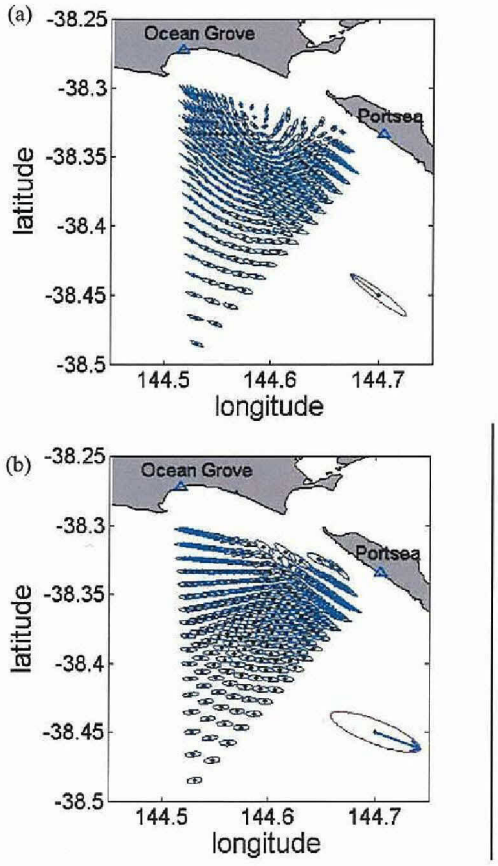

Fig 8 Variability ellipses of currents and wind under (a) long fetch (b) short fetch condition. Wind variability ellipse is at the right bottom, arrow represents dominant wind direction

of the ellipses represents the principal direction along which currents and wind vary mostly during the period. The eccentricity values over entire area are close to one, implying nearly rectilinear currents. The length of the major axis represents the speed of the current. It can be seen that characteristic spatial pattern is quite different for different fetch conditions. For each condition, the characteristics of the ellipses vary with location. A detailed study has been done on current response at the southern points where the response is nearly uniform (Mao and Heron 2006).

To establish a model for the current response to wind over the entire area, we have to establish the relation between current at each grid point and the wind for each section corresponding to wind direction: One is the direction relation and the other is the ratio of wind-generated current speed to wind speed. The direction of both current and wind can be approximated by the direction of their major axis. Therefore, the angle α between the current and the wind is obtained by the variability ellipse analysis for different time sections.

After α is ascertained for each grid point and each time section, the ratio λ of wind-generated current speed to the wind speed, and the assumed constant current $\overrightarrow{V_0}$ can be obtained through a least square fitting process.

$$\overrightarrow{V} = \lambda \cdot \overrightarrow{W} \cdot (\cos(\alpha) + \sin(\alpha)) + \overrightarrow{V_0} \qquad (1)$$

Where $\overrightarrow{V}$ is the filtered observed currents, $\overrightarrow{W}$ is the filtered wind vector. λ and $\overrightarrow{V_0}$ are derived for each time section. Together with α, the wind generated currents can be reconstructed with these three parameters.

Fig 9 shows the comparison of reconstructed wind-generated current and the observed total current at a grid point. Sections with no wind-generated current records correspond to period when the wind speed is less than 3m/s. It can be seen that reconstructed wind-generated currents cover most of the low frequency variation in the current.

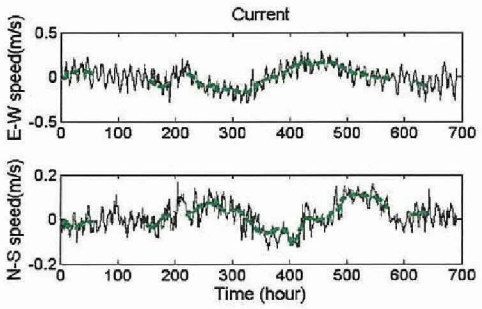

Fig 9 Typical records of observed current (line) and reconstructed wind-generated current (thick dashed line), sections with no records of reconstructed wind-generated current correspond to period when the wind speed is less than 3m/s

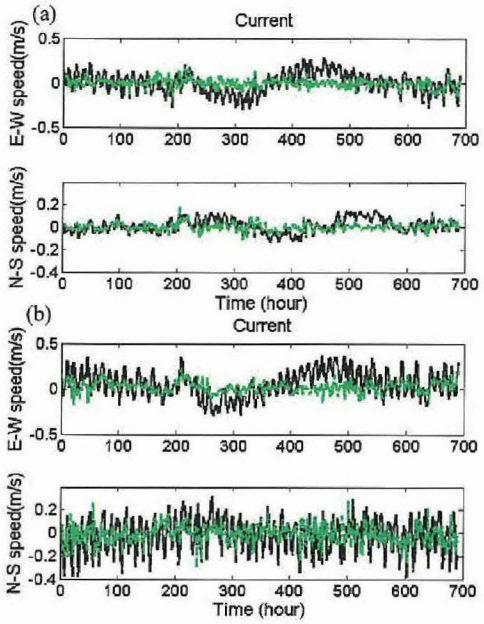

Fig 10 Comparison of the observed current (dark line) with the residual current (light dashed line) (a) in the southern part (b) near the entrance of the bay

Superimposing the tidal current derived from tidal analysis on the wind-generated current, we obtain the reconstructed current. Finally, the residual current is obtained by subtracting the reconstructed current from the observed current. Fig 10 shows the comparison of residual currents and the observed currents at the same two typical grid points as in Fig 2, one in the southern part (Fig 10 (a)), the other near the entrance of bay (Fig 10 (b)). It can be seen in Fig 10 that most of the current variability is explained by tides and winds with quite noisy residuals left. The residual is small compared to the observed currents, especially in the E-W direction. Due to more high frequency fluctuation of wind in the N-S direction, more high frequency fluctuations occur in the currents in the N-S direction and therefore it is left in the residual.

6. Conclusion

So far, we have demonstrated the process for establishing a physical empirical model for surface current prediction using the historical current records from HF radar. This is achieved by exploring the respective influence of different driving forces for the current and a linear superposition of the current generated by each force. In our study area, we find that winds and tides are the main driving forces. In areas where more factors, such as strong geostrophic current and up-welling or sinking are acting as the driving force, the model can be adapted to take those factors into account.

The reliability of reconstructed currents increases with the length of current record. Due to the limitation of the relatively short record length, the parameters α, λ and $\overline{V_0}$ were derived for only a few wind directions. If the records of surface current velocity are long enough that the condition includes wind from all directions, with long enough current records for each wind direction, the empirical model will be complete and can be used to predict surface currents once the wind is known. The model predictions are as good as the tide and wind forecasts that are put into it, and at the moment the limit is up to about 7 days. This model has the advantage of short computing time for current prediction once the model is established; therefore it has great potential in many urgent tasks in the coastal area, such as search and rescue operations and monitoring spilled oil from ships.

References:

Huang, N. E. (1979) On surface drift current in the ocean. *Journal of Fluid Mechanics*, Vol. 91, 191-208.

Lewis, D. M. and Belcher, S. E. (2003) Time-dependent, coupled Ekman boundary layer solutions incorporating Stokes drift. Dynamics of Atmosphere and Oceans, Vol. 37, 313-351.

Mao, Y. and Heron, M. (2006) The influence of fetch on the response of surface currents to wind. *Journal of Physical Oceanography*, accepted.

Kirwan, A. D., McNally, G., Pazan S. and Wert R. (1979) Analysis of surface current response to wind. *Journal of Physical Oceanography*, Vol. 9, 401-412.

Pawlowicz, R., Beardsley, B., and Lentz, S. (2002), Classical tidal harmonic analysis including error estimates in MATLAB using T-TIDE, *Computers and Geosciences,* Vol. 28, 929-937.

Polton, J. A, Lewis D. M. and Belcher, S. E. (2005) The role of wave-induced Coriolis-Stokes forcing on the wind-driven mixed layer. *Journal of Physical oceanography*, Vol. 35, 444-457.